Chapter 7
Harnessing of 2D Carbon-Based Heterostructures as a Photocatalyst Towards Wastewater Treatment

Sujoy Kumar Mandal, Sumit Mandal, and Debnarayan Jana

7.1 Introduction

In the world we have today with growing industrialization, water pollution has already surpassed the danger line. The released excess dyes and harmful chemicals into the river, lakes, etc. not only affects human life but also the entire biosphere—plants and organisms living in these water bodies [1]. Throughout the world, pure drinking water is becoming scarce day by day. According to the prediction by the World Bank, half of the world's population will be living in water-stressed areas by 2025. Furthermore, a 2020 study published in The Lancet by researchers funded by the Global Burden of Disease Study projects that the world population will peak in 2064 at 9.7 billion [2]. In the recent decades, a lack of drinkable water has become a global challenge for civilization. Unregulated and uncontrolled human population and industrialization growth in the current era have disrupted the natural purification process, which has ultimately led to the scarcity of potable water. Treatment of wastewater and its reusability is a critical issue from both an environmental and a social standpoint, and it must be approached with caution to alleviate the age-old problem of water pollution. Over the few decades, various strategies based on biological, mechanical, electrochemical oxidation, and chemical processes have been initiated for the treatment of contaminated water [3–6]. But, given the lesser efficiency of these processes, there arose advanced oxidation processes (AOPs) as superior alternatives to all these processes [7, 8]. Among them, advanced oxidative processes (AOP) have gained the trust of the scientific community as a promising scheme for the destruction of organic contaminants in wastewater. In reality, in this process, highly reactive species, i.e.,

S. K. Mandal · D. Jana (✉)
Department of Physics, University of Calcutta, 92, A.P.C. Road, Kolkata 700009, India
e-mail: djphy@caluniv.ac.in

S. Mandal
Department of Physics, Vidyasagar College, 39, Sankar Ghosh Lane, Kolkata 700006, India

K. Mohanty et al. (eds.), *Graphene and its Derivatives (Volume 2)*, Materials Horizons: From Nature to Nanomaterials, https://doi.org/10.1007/978-981-99-4382-1_7

hydrogen peroxide (H_2O_2), hydroxyl radical ($^{\cdot}OH$), and superoxide radical ($\dot{O}_2^-$), are generated which act as the active agents for the mineralization of organic compounds or contaminants in water [9]. However, improvements in the efficiency of these processes, such as the ability to properly use natural resources like solar radiation, may assist to make them more cost-effective [10]. In this regard, among AOPs, heterogeneous photocatalysis has become the most efficient method with the efficacious degradation ability of a wide range of organic contaminants into CO_2, water, and some readily biodegradable mineral acids. When Akira Fujishima and Kenichi Honda discovered the electrochemical photolysis of water in 1972, it ushered in a new era in photocatalysis research [11, 12]. Since then, numerous semiconductor oxides like titanium dioxide (TiO_2), zinc oxide (ZnO), molybdenum disulphide (MoS_2), and perovskite oxides like bismuth tungstate (Bi_2WO_6) and their various form of heterostructures have been probed as an efficient photocatalyst [13–16]. In this book chapter, we will first focus on describing the fundamental mechanisms of photocatalysis, including the essential factors for an efficient photocatalyst. The later sections will cover the important properties of graphene and graphene derivatives (i.e., graphene oxide (GO) and reduced graphene oxide (rGO)), and their role in heterogeneous photocatalysis will be showcased, followed by a brief timeline of the development of graphene-semiconductor heterogeneous photocatalyst towards the decomposition of hazardous chemicals in the aqueous medium. And finally, we will wrap up this book chapter with a summary of the major challenges and the prospects with graphene-related heterostructure in the realm of wastewater treatment.

7.1.1 Photocatalysis and Its Mechanism

Photocatalysis is defined as the stimulation of a chemical reaction on the active surface of a catalyst by a sufficient amount of light energy (i.e., either UV or visible). Photocatalyst is the name given to this sort of catalyst. The overall process in photocatalysis occurred in five independent steps: (i) mass transfer of the reaction from the bulk phase (either aqueous or gaseous), (ii) adsorption of the reactants, (iii) photocatalytic reaction, (iv) product desorption, and finally (v) mass transfer of the products from the interface to the bulk phase [17]. When a semiconductor (SC) is excited with energy greater or equal to its bandgap (E_g) energy, electron (e^-)–hole (h^+) pairs are generated, where, e^-_{CB} is the electron in the conduction band (CB) and h^+_{VB} is the hole in the valence band (VB). The photogenerated electron–hole pairs can migrate to the semiconductor and then be adsorbed by the active surface of the photocatalyst.

The positive hole can oxidize the organic and inorganic pollutants directly, but in most cases, it is caused by the production of hydroxyl ($^{\cdot}OH$) radicals. The $^{\cdot}OH$ radical is formed by the direct oxidation of adsorbed water (i.e., hydroxide ion, OH^-) on the surface of the semiconductor catalyst by the valence band hole. Also, the photogenerated conduction band electron indirectly produces $^{\cdot}OH$ radicals. The redox potential of the conduction band electron is −0.52 V which is negative enough to reduce dissolved oxygen to superoxide ($\dot{O}_2^-$) radical [18]. The superoxide radical

reacts further with water to form a hydroxyl radical. Furthermore, the generated superoxide radical is very reactive, capable of immediately oxidizing colour or any other harmful molecule before decomposing into CO_2 and H_2O. Finally, the dyes or organic contaminants are degraded into environmental-friendly chemicals by these extremely reactive radicals. The overall reaction can be summarized as follows [19]:

$$SC \xrightarrow{hv} SC\left(e_{CB}^{-} + h_{VB}^{+}\right)$$

From valence band hole

$$h^{+} + H_2O \big/ OH^{-} \rightarrow {}^{\cdot}OH + H^{+}$$

From condition band electron

$$e_{CB}^{-} + O_2 \rightarrow \dot{O}_2^{-}$$

$$\dot{O}_2^{-} + H_2O \rightarrow H\dot{O}_2 + OH^{-}$$

$$2e^{-} + H^{+} + H\dot{O}_2 \rightarrow \dot{O}H + OH^{-}$$

$$h^{+}\ or\ \dot{O}_2^{-} or \dot{O}H + Dye \rightarrow CO_2 + H_2O$$

The oxidation–reduction process has been illustrated schematically in Fig. 7.1.

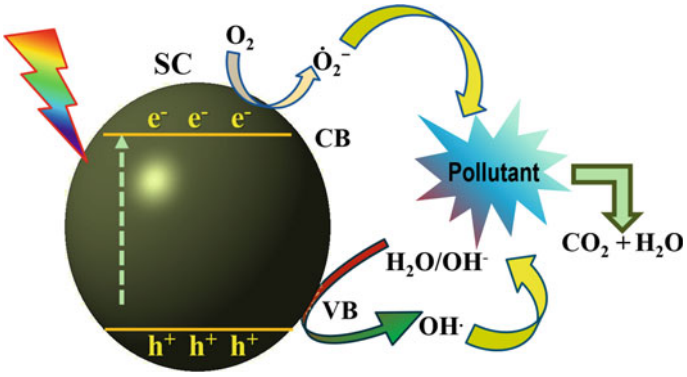

Fig. 7.1 Schematic representation of the mechanism of photocatalysis by a semiconductor photocatalyst

7.1.2 Essential Factors Involved in a Semiconductor Photocatalyst

Fundamentally, the efficiency of a semiconductor as a photocatalyst depends mainly on three key factors: (i) bandgap, (ii) conduction band and valence band position, and (iii) charge carrier dynamics, such as charge carrier mobility, diffusion length and lifetime as well as the rates of surface charge recombination and interfacial charge transfer process. Besides this, the photocatalytic degradation efficiency also depends on the surface area, as photocatalysis is a complete surface phenomenon [20].

Bandgap determines whether a photocatalyst will be activated with ultraviolet (UV) or visible irradiation. Some of the semiconductor material's bandgap lies in the UV region. Like, bare ZnO (E_g = 3.37 eV), TiO_2 ((E_g = 3.31 eV), and ZnS (E_g = 3.67 eV) play the role of a photocatalyst only under the irradiation of UV light [21–23]. Our solar spectrum, on the other hand, has just 4–5% UV irradiation, with about 44% in the visible spectrum and the rest in the infrared. As a result, an additional energy source is required to activate the photocatalyst. To overcome this type of limitation, several approaches viz. doping to semiconductor heterostructure formation by coupling with a secondary substance (like noble metal, non-metal, other semiconductors, carbon-based materials, and so on) have been implemented. On the other hand, some semiconductor materials, like SnS_2 (E_g = 2.24 eV), MoS_2 (E_g = 1.29 eV), and CdS (E_g = 2.40 eV), can be activated as a photocatalyst with visible or sunlight irradiation owing to the presence of bandgap in the visible region [24–26]. But, for these types of materials, photocatalytic efficiency is also limited due to the constraint of other two factors like band position and charge carrier dynamics. In this case, heterostructure formation also plays a crucial role to make this photocatalyst a fruitful remedy for wastewater treatment.

However, the band edge position of the semiconductor is the most important for use as a photocatalyst. The energies of the conduction (E_{CB}) and valence (E_{VB}) bands govern the electron injection ability of the material at the surface. Also, the ability of a semiconductor to undergo photoinduced charge carrier transfer to adsorbed species on its surface is governed by the band energy positions of the semiconductor and the redox potentials of the adsorbed species. Therefore, the knowledge of the absolute positions of E_{CB} and E_{VB} band edges is indispensable to exploring the potential applications of the concerned semiconductor as an efficient photocatalyst. The energy level at the bottom of the conduction band actually determines the reduction potential of photoelectrons and the energy level at the top of the valence band determines the oxidizing ability of photogenerated holes, each value reflecting the ability of the system to promote reductions and oxidations, respectively [27].

When a semiconductor is in contact with the ionic interactions at the interface of the two phases, this leads to electrostatic equilibrium within the material. Particularly at the semiconductor/electrolyte interface, electrons flow from the phase of more negative Fermi energy (E_F) to the other to attain equilibrium, in which the semiconductor E_F matches the electrolyte $E_{F,\,redox}$. This causes the formation of a space charge layer (SCL) within the semiconductor phase associated with the bending of

the band edges in the semiconductor. The magnitude and direction of band bending can be adjusted by an externally applied potential. The externally applied potential known as flat band potential (E_{FB}) diminishes the band bending in a semiconductor, in contact with the electrolyte. Hence, the E_{FB} determines the energy of two charge carriers at the interface [28].

From the thermodynamic point of view, adsorbed molecules can be reduced photocatalytically by conduction band electrons if they have redox potentials lower (more positive) than the flat band potential of the conduction band. That can be oxidized by valence band holes if they have redox potentials higher (more negative) than the flatband potential of the valence band [29–31]. However, the primary criteria to get a good semiconductor photocatalyst for organic compound degradation are the redox potential of the $H_2O/^{\cdot}OH$ ($HO^- = {}^{\cdot}OH + e^-$, $E_0 = -2.8$ V) [32] couple lies within the bandgap domain of the material and the stability over prolonged periods of time. The bandgap and the corresponding band edge positions of some frequently used semiconductors are presented in Fig. 7.2 [33].

An ideal photocatalyst should possess the following features: (i) photoactive, (ii) can utilize visible and/or near-UV light, (iii) biologically and chemically inert, (iv) photo-stable (not prone to photo-anodic corrosion), (v) inexpensive, and (vi) non-toxic. We must study the basic principles of photocatalysis to increase photocatalytic performance. The photocatalytic behaviour is also affected by the temperature and pH of the solution. Various ways for producing an effective semiconductor heterostructure photocatalyst have been developed throughout the decades and will be reviewed in the next section.

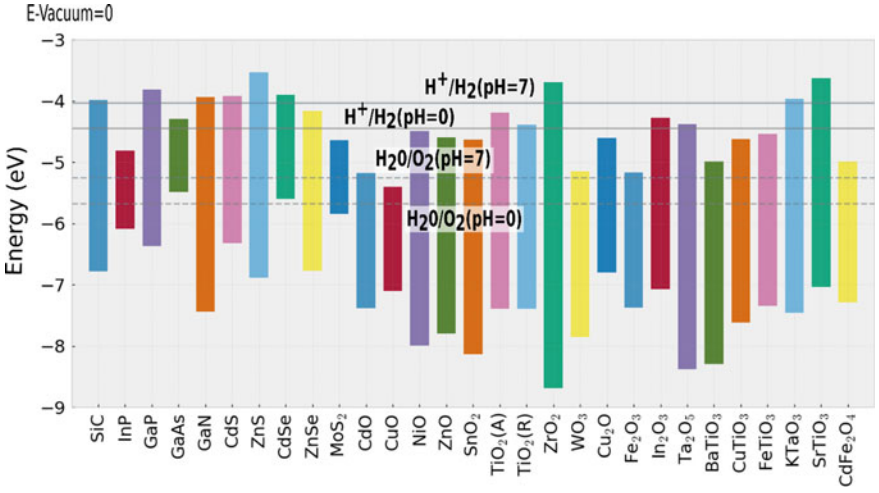

Fig. 7.2 The bandgap and the corresponding band edge positions of some frequently used semiconductors [reproduced with permission from Ref. [34]

7.1.3 Historical Journey of Semiconducting Photocatalysts

The earliest venture in photocatalysis is credited to the German chemist Dr. Alexander Eibner when for the first time in 1911, he integrated the concept of the illumination of zinc oxide (ZnO) on the bleaching of the dark blue pigment, Prussian blue [34]. Bruner and Kozak also proposed the hypothesis of oxalic acid degradation in the presence of uranyl salts under light about this time [35, 36]. In 1913, Landau wrote an article that described the concept of photocatalysis through the invention of actinometric measurements, which are the foundation for calculating photon flux in photochemical processes [35, 37]. However, in the 1970s, the global oil crisis stimulated the worldwide research community to find an alternative source of energy. As a result, a breakthrough in photocatalysis research occurred in 1972, when Akira Fujishima and Kenichi Honda discovered the electrochemical photolysis of water [38]. In their work, the ultraviolet light was absorbed by the TiO_2 electrode, and electrons would flow from the TiO_2 electrode (anode: site of oxidation reaction) to the platinum electrode (cathode: site of redox reaction), with hydrogen production occurring at the cathode. After this seminal work, extensive research has been conducted utilizing a variety of semiconductor photocatalysts to investigate whether hydrogen may be produced from a clean and cost-effective source [39, 40]. These kinds of light-harvesting applications for semiconductor colloidal solutions have been explored for decades as a new material for solving the global energy issue and saving the environment. Wide-bandgap semiconductors, such as TiO_2 and ZnO, have generally proven to be better photocatalysts than low-bandgap materials, such as nickel oxide (NiO) and cadmium sulphide (CdS), owing to the former's higher free energy of photogenerated charge carriers and the latter's inherently low chemical and photochemical stability. Low-bandgap semiconductors, on the other hand, make greater use of solar radiation, lowering the cost of additional energy sources. Whereas wide bandgap semiconductors need an extra energy source to play the role of an activated photocatalyst. Furthermore, limited absorption spectra, low photon quantum efficiency, photocorrosivity, and rapid recombination of photogenerated electron holes are all disadvantages of bare semiconducting photocatalytic processes in practical applications.

In recent years, a great deal of work has gone into the creation of more efficient photocatalysts with higher quantum efficiency and better sensitivity to the visible spectral region. Promising results in this direction have been obtained with the use of several methods aiming at the modification of electronic and optical properties of semiconductors, including novel metal deposition, dye sensitization, doping with transition metals or non-metallic elements, use of composite semiconductor photocatalysts, semiconductor–carbon (S-C) heterostructure, and Z-scheme or multicomponent heterostructure. Among all types of composite formation, S-C heterostructure (S-C) plays an important role in heterogeneous photocatalysis. In an S-C heterostructure, different forms of carbon like activated carbon, carbon nanotube (CNT), and graphene and its derivatives like graphene oxide (GO) and reduced graphene oxide have been extensively used as a photocatalyst.

7.2 Photocatalysts in the Realm of Wastewater Treatment

Because photocatalysis is a surface phenomenon, researchers initially concentrated on the creation of different nanostructures with a larger surface-to-volume ratio. Moreover, the valence band and conduction band of the semiconductor change into discrete energy levels as a result of quantum size formation, which means that the valence band electric potential changes more positively; otherwise, the conduction band electric potential changes more negatively. The oxidation–reduction potential of electrons and holes is then raised, resulting in an increase in the oxidation activity of nanosized photocatalysts. The bandgap of ZnO and ZnS can be narrowed by doping with metal impurities such as Cu and Mn [41–44]. The incorporation of dopant atoms into the semiconductor crystal lattice introduces intermediate energy levels or trap states within the intrinsic semiconductor, which lowers the energy requirement for the photoexcitation of electrons as well as enhances the electron–hole pair charge separation [45]. As a result, the photocatalytic activity is improved. Inappropriate metal ion dopants, on the other hand, might behave as a recombination centre, resulting in reduced photocatalytic activity [46]. Non-metal doping, such as nitrogen (N), carbon (C), or sulphur (S), can also be used to restrict the bandgap energy to the ultraviolet–visible range by pushing the VB energy upward (S) [47–57]. Due to the nature of p-type doping, N and C doping can generate vacant states above the Fermi level (EF) and shift the CB into a lower energy region, resulting in a narrowing of the bandgap [58, 59]. Liu et al., for example, created a hierarchical flower-like C-doped ZnO superstructure with improved photocatalytic activity, which they ascribe to the action of doping carbon atoms into the ZnO lattice [60]. For further improvement of the photocatalytic activity of zinc-based materials, researchers have developed different types of semiconductors heterostructures. Typically, these heterostructures are classified into four types as follows: (a) semiconductor–metal heterostructure, (b) semiconductor–semiconductor heterostructure, (c) semiconductor–carbon heterostructure, and (d) multicomponent (comprising metals and semiconductors) heterostructure.

A combination of metal and semiconductors can be a more efficient photocatalyst for capturing solar light than either component alone. In most cases, n-type semiconductors are employed to make these heterostructures. A Schottky barrier is generated between the metal and semiconductor junctions, which can act as an effective electron trapping and inhibit electron–hole recombination, increasing photocatalytic behaviour. Several research groups, notably Kang et al. [61], Vaiano et al. [62], and Chen et al. [63], have synthesized Ag-modified ZnO towards increased photocatalytic performance. However, there is a concern here as well: metal is hazardous to the environment. Furthermore, correct coupling of a semiconductor with another semiconductor with different bandgap energy reduces the effective bandgap energy, allowing for more efficient charge separation, faster charge transfer to the catalyst, and a longer charge carrier lifespan. Jung et al. for example, found that flower-like CuO–ZnO heterostructure nanowires (NWs) exhibit higher photocatalytic activity than bare ZnO and CuO in the breakdown of acid orange 7 (AO7) [64]. Under visible irradiation, Bharathia et al. discovered that a 5 Wt% CuO-loaded CuO/ZnO

heterostructure had the best degradation performance, with about 96.57% degradation efficiency towards methylene blue (MB) dye [65]. Using $ZnOCu_2S$ with ZnS interlayer heterostructure, Ranjith et al. obtained 93.47% degradation of rhodamine B (RhB) dye within 75 min of sun irradiation [66].

7.3 Graphene: The Game Changer

Graphene has unique properties like high surface area possessing a two-dimensional (2D) structure of sp^2 hybridized carbon atoms has drawn tremendous attention to the scientific as well as engineering community. In 2004, two researchers at the University of Manchester, Professor Andre Geim and Professor Kostya Novoselov, first discovered graphene through the simple exfoliation of graphite by scotch tape [67]. The unique one-atom-thick 2D honeycomb lattice structure of graphene not only makes it the thinnest and strongest material in the universe, but also endows it with many excellent chemical and physical properties. The excellent features of graphene, like good adsorption, [68] good electrical conductivity (2000 S m^{-1}), superior carrier mobility with little scattering at room temperature (200,000 cm^2 V^{-1} s^{-1}), [69, 70] extremely high theoretical specific surface area (2630 m^2 g^{-1}), [71] excellent environmental compatibility, and cost-effective production, [72] made it a suitable choice for photocatalytic applications. Moreover, due to these superior properties, 2D graphene exhibits more promising applications in optical, electronic, biological, and catalytic fields than other carbon allotropes (i.e., 0D fullerenes, 1D nanotubes, and 3D graphite) [73, 74].

However, graphene derivatives like graphene oxide (GO) and reduced graphene oxide (RGO) have acquired great interest than graphene as a superior support material for the formation of nanocomposites with metal oxide and sulphides towards photocatalytic wastewater management. Formation of graphene nanocomposites provides several benefits: (i) prevention of stacking of graphene sheets: carbon atom within the graphene structure possesses p bond oriented out of plane making them vulnerable to stack over one other, (ii) improvement of conductivity, (iii) reduction of photogenerated electron–hole pair recombination, and (iv) improvement of charge carried dynamics [75, 76].

7.3.1 Importance of Graphene Oxide (GO) in Photocatalysis

Talking about the graphene family, GO has garnered ample attention as an effective adsorbent due to its extreme hydrophilicity, ultrahigh theoretical surface area [71], and plentiful oxygen atoms on the graphitic backbone of graphene oxide in the form of epoxy, hydroxyl, and carboxyl groups which protrude from its basal planes and edges [77, 78]. These functional groups can strongly interact with a variety of organic materials and thus yield new materials that can be effectively tailored for

the adsorptive removal of diverse water pollutants [79]. Also, the presence of these hydrophilic groups results in the stable dispersion of GO in aqueous solutions. It also disperses in several organic solvents.

Graphene oxide has a limited electrical conductivity, which causes it to behave as either insulating or semi-conductive depending on the degree of oxidation. In 1859, Oxford scientist Benjamin C. Brodie created graphite oxide by treating graphite with a solution of potassium chlorate and fuming nitric acid [80]. He claimed to have synthesized "paper-like foils" with a thickness of 0.05 mm. Hummers and Offeman created the Hummers' technique in 1957, which uses a combination of sulphuric acid H_2SO_4, sodium nitrate $NaNO_3$, and potassium permanganate $KMnO_4$ with graphite powder and is still extensively used today with some modifications [81].

7.3.2 Importance of Reduced Graphene Oxide (RGO) in Photocatalysis

The reduction of graphene oxide is another graphene derivative with properties that are similar to graphene. Reduced graphene oxide (RGO) is a kind of graphene oxide that has had its oxygen concentration reduced by chemical, thermal, and other means. RGO is often less defect-free and of lower grade than graphene made straight from graphite. Residual oxygen and other heteroatoms, as well as structural flaws, are seen in reduced graphene oxide (RGO). Due to the relative simplicity of producing substantial quantities of graphene at a cheap cost, reduced GO is typically a logical and understandable choice for applications that require huge volumes of material.

When compared to broadband semiconductors, RGO has a narrow bandgap. As a result of its ability to absorb more photons than semiconductors, a huge number of electron and hole pairs are formed inside the material. RGO's high electrical conductivity allows it to transport photogenerated charge carriers to the semiconductor's conduction band, resulting in a large population of charge carriers in the composites that react with surface-absorbed O_2 and H_2O. As a result, on the surface of the nanocomposites, a huge number of superoxide and hydroxide radicals develop, which destroy the hazardous dyes [82]. Because graphene has a large surface area and a dense structure, its composites naturally minimize the time it takes for electron–hole pairs to recombine, enhancing its photocatalytic activity for the destruction of hazardous dyes. Pure semiconducting nanostructures have lower photocatalytic activity than composite formations of RGO and semiconductor oxides. Figure 7.3 shows a schematic representation of the differences between graphene, GO, and RGO.

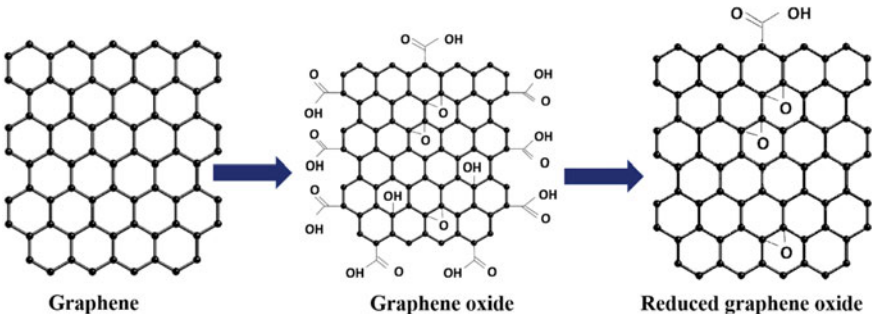

Fig. 7.3 Schematic representation of the structure of graphene, graphene oxide, and reduced graphene oxide [reproduced with permission from Ref. 82]

7.3.3 GO-Based Semiconductor Photocatalysts

The formation of heterostructure of semiconductor materials with GO can be effectively used as a visible light-driven photocatalyst in wastewater treatment basically in organic dye degradation. The presence of active groups such as carbonyl, epoxy, and hydroxyl groups on the surface of graphene oxide enables it to interact with a wide variety of molecules and thus can undergo surface modification. Recently, numerous studies devoted to the utilization of self-assembled metal oxides and metal sulphide nanomaterials on GO for the removal of different water pollutants, have been reported. A major advantage of GO is that it can be used to facilitate electron transfer which consequently diminishes the probability of electron (e^-)–hole (h^+) pair recombination in such semiconductor photocatalysts. Fabrication of such materials with GO results in an increase in the absorption of light as well as the surface area of the composites. Thus, the photocatalytic activity of the composite materials increases dramatically. Therefore, the use of GO as a supporting material along with various other semiconductors as stable, recyclable, and fully efficient photocatalysts has been found to be a challenging area of research. For example, recently Lin et al. [83] have synthesized GO/TiO_2 heterostructure and studied the photocatalytic degradation of methylene orange (MO) dye. They have observed that GO/TiO_2 composite shows better degradation ability than bare GO or TiO_2 nanomaterials. Moreover, GO/TiO_2 composite shows better thermal stability. The comparison of photocatalytic degradation of MO dye with respect to the time of GO, TiO_2, and GO/TiO_2 composites in 48-W UV light irradiation is represented in Fig. 7.4.

Similarly, Durmus et al. [84] used a GO/ZnO nanocomposite as a photocatalyst to break down basic Fuchsin Dye with the help of UV light exposure. In this case, the GO/ZnO combination outperforms both ZnO and GO in terms of deterioration. The degradation rate constants for GO, ZnO, and ZnO/GO composite were found to be 8.52×10^{-4}, 2.92×10^{-3}, and 8.45×10^{-3} min^{-1}, respectively. In the instance of GO/ZnO, photonic irradiation excites electrons in ZnO to the conduction band, whereas holes develop in the valence band. The fact that GO works as a photoexcited

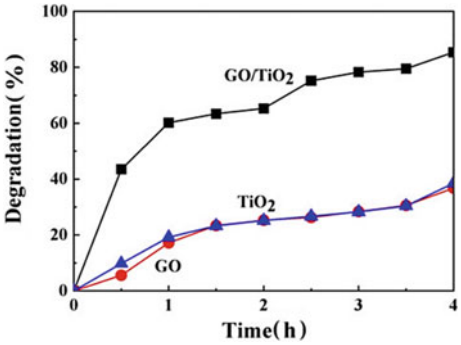

Fig. 7.4 Photocatalytic degradation of GO, TiO_2, and GO/TiO_2 composites in 48-W UV light irradiation [reproduced with permission from Ref. 83]

electron acceptor relates to the fact that excited electrons of ZnO move from the conduction band of ZnO to GO. As a result, photoelectron–hole pair recombination decreases, allowing a sufficient quantity of reactive radicals to be produced. Ahmad et al. [85] developed p-type NiO/n-type GO photocatalysts for the degradation of organic pollutants and conducted tests on the photocatalytic degradation of methylene blue (MB) as a test pollutant at room temperature using UV–Vis light irradiation. The greatest catalytic activity was found in p-type NiO/n-type GO nanocomposites with 65% GO. In approximately 50 min of irradiation, the photocatalyst dissolved about 97% of the original MB dyes. The construction of a p-type NiO and n-type GO heterojunction is critical for greater separation of photogenerated electrons and holes, as well as a high level of recombination inhibition, resulting in increased photocatalytic activity. Figure 7.5 depicts a p-type NiO/n-type GO nanocomposite photocatalyst in schematic form.

On the other hand, visible light-activated photocatalyst may be seen in the composite synthesis of GO with a low-bandgap material. Gao et al. [86] developed a GO/CdS heterostructure and studied the photocatalytic degradation of Acid Orange

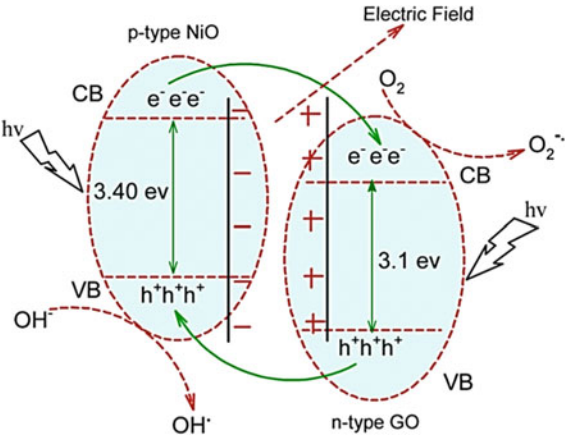

Fig. 7.5 Schematic representation of p-type NiO/n-type GO composite photocatalyst [reproduced with permission from Ref. 85]

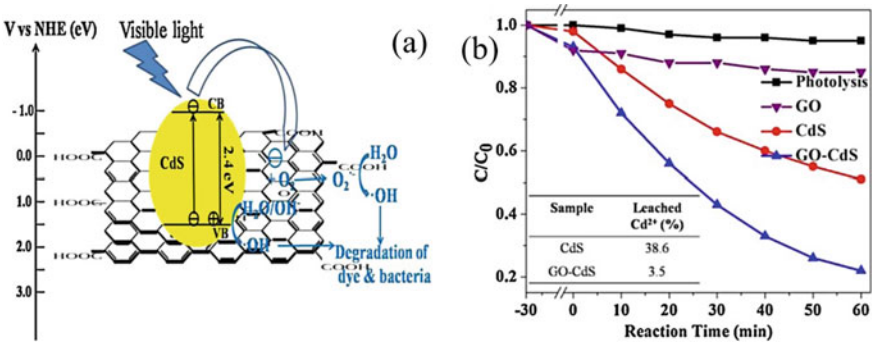

Fig. 7.6 **a** schematic illustration of charge transfer and formation of ˙OH, **b** the changes of AO7 concentration with the irradiation time [reproduced with permission from Ref. 86]

7 (AO7) under visible light irradiation as well as the antibacterial activity of these materials. GO–CdS has a substantially better efficiency in AO7 dye degradation and Cr^{6+} reduction than pure CdS. Furthermore, GO–CdS composites are highly effective against Gram-negative E. coli as well as Gram-positive B. subtilis. Furthermore, throughout the photodegradation process, the composites are photo-stable. Figure 7.6 shows a schematic representation of charge transfer and generation of ˙OH, as well as variations in AO7 concentration during photodegradation.

Many research groups have reported the fabrication of some GO-based semiconductor materials to improve photocatalytic activities towards wastewater management to a significant extent by coupling GO with various materials such as TiO_2 [83], ZnO [87], CuO [88], SnO_2 [89], Fe_2O_3 [90], WO_3 [91], Bi_2O_3 [92], $BiVO_4$ [93], Ag_3PO_4 [94], and many others.

7.3.4 Fabrication of GO-Based Ternary Composites

The synergistic impact of two semiconductor materials and graphene oxide sheet modification on the ternary composites' increased photocatalytic activity has piqued our curiosity. The ternary composite is projected to have better light efficiency due to the synergistic impact of the semiconductor's light sensitivity and GO's quicker electron transfer capabilities. Cui et al. [95] have developed a unique triple-component TiO_2/Ag_3PO_4/graphene oxide (TiO_2/Ag_3PO_4/GO) photocatalyst with dual-channels for the separation of photogenerated charges. Under visible light irradiation, TiO_2/Ag_3PO_4/GO showed higher photocatalytic activity and stability over bare Ag_3PO_4, TiO_2/Ag_3PO_4, and Ag_3PO_4/GO in the degradation of Rhodamine B (RhB) and phenol solutions.

Because the electronic band structures of TiO_2, Ag_3PO_4, and GO are aligned, photogenerated electrons in Ag_3PO_4 can be quickly transferred to GO sheets via an

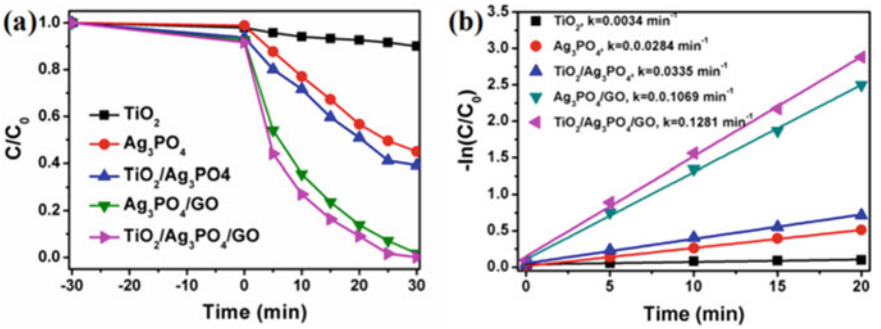

Fig. 7.7 **a** RhB photodegradation as a function of illumination time for TiO_2, Ag_3PO_4, TiO_2/Ag_3PO_4, Ag_3PO_4/GO, and TiO_2/Ag_3PO_4/GO under visible light; **b** the plots of -ln(C/C_0) versus t. where C_0 is the initial concentration of RhB before light irradiation and **c** is the concentration at irradiation time t [reproduced with permission from Ref. 95]

$Ag_3PO_4 \rightarrow$ GO electron transfer channel, whereas photogenerated holes can be transferred to TiO_2's valence band via an $Ag_3PO_4 \rightarrow TiO_2$ hole transfer channel. The dual-channel for photogenerated charge separation at the TiO_2/Ag_3PO_4/GO interfaces finally reduces photogenerated electron–hole pair recombination, resulting in improved photocatalytic activity and stability. Figure 7.7a depicts the RhB dye degradation performance for all composites, whereas Fig. 7.7b depicts the logarithmic plot comprising degradation rate constants.

Various research groups have fabricated several extremely efficient GO-based dual-channel heterostructure ternary composites such as P25/Ag_3PO_4/GO [96], Ag/ZnO/GO [97], ZnO-g-C_3N_4 coupled with GO [98], Ag_2MoO_4/Ag/AgBr/GO heterostructure [99], N-TiO_2/Ag_3PO_4@GO [100], graphitic-C_3N_4/BiOI/GO [101], and Fe_3O_4/Cu-BDC/GO [102], which are successfully utilized as an enhanced photocatalyst.

7.3.5 Fabrication of RGO-Based Binary Composites

Reduced graphene oxide has a narrow bandgap compared to wide band oxides; so it absorbs more photons than oxides. As a consequence, a large number of electron and hole pairs are created inside the material. RGO can transfer the photogenerated charge carriers to the conduction band of the semiconductor, resulting in a huge population of charge carriers in the composites, reacting with surface-absorbed O_2 and H_2O. As a result, a large number of superoxide and hydroxide radicals are formed on the surface of the nanocomposites which degrade the toxic dyes. Mandal et al. [82] used ZnO quantum dots and GO solution as precursor materials for the solvothermal synthesis of ZnO/RGO nanocomposite photocatalyst. Effective photoluminescent quenching is found as a result of composite production and bandgap decrease. Within 25, 15,

and 30 min, their optimized ZnO/RGO composite successfully removed Safranin O, Methylene Blue, and Rhodamine 6G dyes from the aqueous solution. The purpose of RGO in the composite is to prevent nanoparticle aggregation by increasing the number of active sites. It also has a higher capability for capturing photons and transferring photogenerated electrons to the conduction band of ZnO. As a result, recombination loss is decreased, and a high number of charges become accessible on the ZnO QD surface. Under light irradiation, the massive amount of oxide and hydroxide super radicals formed on the surface of the QD efficiently destroys the dyes. The method of dye photodegradation employing ZnO/RGO composites as a catalyst is shown schematically in Fig. 7.8.

Similarly, Wang et al. [103] used photocatalytic breakdown of phenol in aqueous solution to compare photocatalytic performance of TiO_2 and TiO_2-RGO composites work as a cocatalyst for the quick transfer of photogenerated electrons from TiO_2, resulting in less recombination and increased photocatalytic activity. In the case of 1 wt% RGO, there is a significant increase in photocatalytic activity. Furthermore, as compared to bare TiO_2 nanomaterial, synthesized is less photocorrosive. The photogenerated electrons on the conduction band of TiO_2 may efficiently decrease oxygen via the RGO nanosheets when exposed to UV light. The RGO nanosheets operate as a cocatalyst in this situation, allowing for the quick transfer of photogenerated electrons from TiO_2, resulting in a decreased recombination rate and increased photocatalytic activity. Furthermore, given the enrichment of phenol molecules on the surface of RGO nanosheets from solution and the strong coupling of TiO_2 nanoparticles and RGO, it is thought that photogenerated holes on the valence band of TiO_2 can easily transfer to the phenol molecules on the RGO surface via holes or $^{\cdot}OH$ resulting in rapid decomposition. Figure 7.9 schematically depicts the photogenerated charge behaviour at the interface of TiO_2 and RGO.

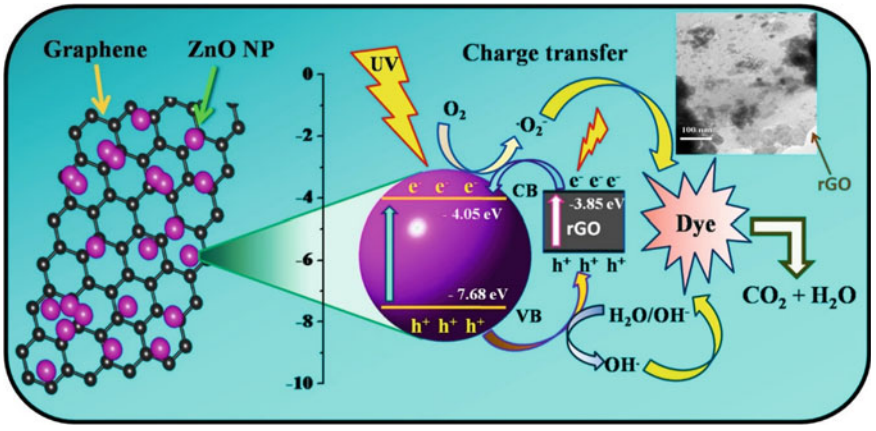

Fig. 7.8 Schematic diagram showing the mechanism of the photodegradation of dye using ZnO/RGO composites as a catalyst [reproduced with permission from Ref. 82]

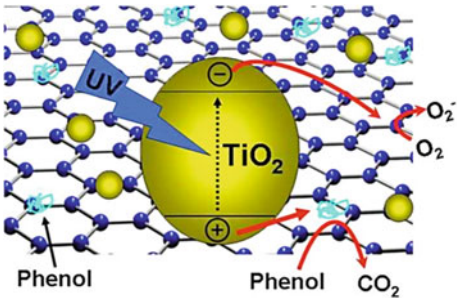

Fig. 7.9 Schematic diagram for illuminating the charging behaviour at the interface of TiO_2 and RGO [reproduced with permission from Ref. 103]

Over the decade, many researchers have synthesized ZnS/RGO [104], Fe_2O_3/RGO [105], $ZnSnO_3$/RGO [106], RGO/SnO_2 [107], SnS_2/RGO [108], and many more and effectively used with an efficacious photocatalytic behaviour towards the decomposition of organic contaminations in aqueous solution.

7.3.6 Fabrication of RGO-Based Ternary Composites

The production of several highly efficient RGO-based dual-channel heterostructure ternary composites, similar to GO, has been the subject of research. Anjaneyulu et al. [109] recently used a ternary nanocomposite composite of MoO_3/Fe_2O_3/RGO as an effective visible light-driven photocatalyst for the degradation of MB dye. The photoelectrons generated in the conduction band (CB) of Fe_2O_3 are transported to the CB of MoO_3 due to the creation of heterojunction. Meanwhile, the exciting holes in the MoO_3 nanobelts' VB are transferred to Fe_2O_3's VB. Finally, by semiconductor–carbon heterojunction, the produced photoelectrons are collected by the RGO sheets. The huge surface area of the RGO sheets, along with their high electrical conductivity, facilitates the passage of produced photoelectrons to the composite surface, preventing recombination between photoinduced electrons and holes. As a result, enhanced photocatalytic activity is spotted. The mechanism of photocatalysis is represented schematically in Fig. 7.10.

Many RGO-based ternary heterostructures, such as Ag/AgBr/RGO [110], RGO/BiOCl/TiO_2 [111], CdS-TiO_2-RGO [112], ZnO-TiO_2/RGO [113], MoS_2-RGO/ZnO [114], RGO/ZnO/Au [115], RGO/ZnS-MoS_2 [116], RGO/Fe_2O_3/g-C_3N_4 [117], and others, have been successfully employed in water decontamination throughout the previous decade. In photocatalysis, the core–shell structure can also play a significant role.

Ding et al. [118] also created magnetically separable Fe_3O_4@CuO-RGO core–shell heterojunctions and used them as a high-performance photocatalyst for organic dye removal under visible light irradiation. Zhou et al. [119] used a one-step hydrothermal approach to make plasmonic Ag@CdSe-RGO hybrid ternary composites, during which the in-situ nucleation of Ag@CdSe core–shell nanoparticles and

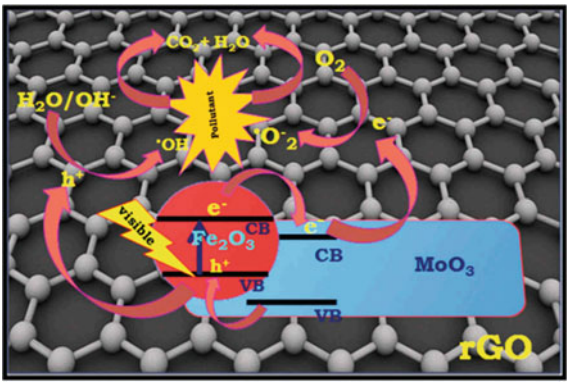

Fig. 7.10 Schematic diagram of a possible photocatalysis mechanism [reproduced with permission from Ref. 109]

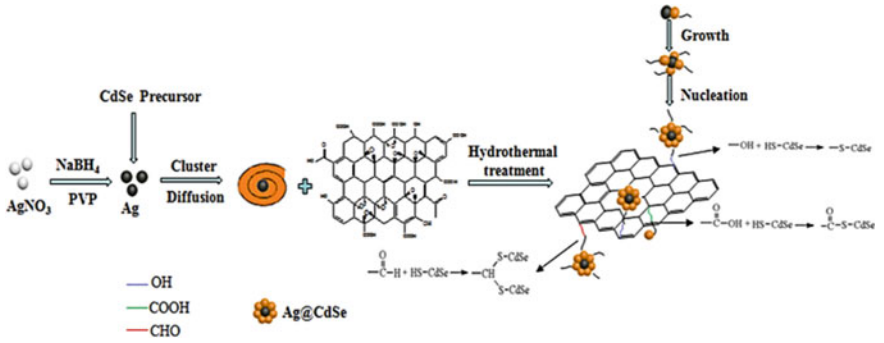

Fig. 7.11 Schematic representation of the proposed mechanism for the formation of the Ag@CdSe-RGO nanoparticles [reproduced with permission from Ref. 119]

the reduction of GO to RGO happened concurrently. Because of the presence of RGO, the improved photocatalytic degradation under visible light irradiation can be attributed to plasmonic enhancement of Ag via charge and energy transfer, which serves to prolong charge separation while also further enhancing the separation of photogenerated e^-–h^+ couples. The hypothesized process for the Ag@CdSe-RGO Nanoparticles production is depicted in Fig. 7.11.

7.3.7 Other Applications of Graphene-Based Photocatalysts

Graphene-based photocatalysts are also effective in hydrogen generation, environmental clean-up, energy storage, CO_2 reduction, sensing, solar cells, and antibacterial activity, in addition to better dye degradation in the aqueous medium. To boost

visible light photocatalytic H_2 generation performance, Abbas Sadeghzadeh-Attar hydrothermally produced $BiVO_4$-TiO_2/RGO heterostructure nanocomposites [120]. At optimum RGO content (3 wt.%) under visible light irradiation, the highest photocatalytic H_2 production rate of 1427.1 μmol. h^{-1} g^{-1} with an apparent quantum yield of 6% at 420 nm was achieved, which was 2.5 and 1.5 times higher than TiO_2 nanotubes (563.5 μmol. h^{-1} g^{-1}) and $BiVO_4$-TiO_2 (915.7 μmol. h^{-1} g^{-1}), respectively. TiO_2 nanoparticles built on GO nanosheets demonstrated strong photocatalytic activity for the photo-reductive reduction of Cr(VI) [121], according to Hu et al.

In the presence of H_2O, Jiang and colleagues [122] developed a PVK-based Z-scheme heterojunction, α-Fe_2O_3/Amine-RGO/$CsPbBr_3$, for high-efficiency CO_2 reduction. Effective Z-scheme electron transfer from α-Fe_2O_3 to $CsPbBr_3$ is produced by carefully regulating the interfacial contact, resulting in increased charge separation and carrier lifespan. When compared to $CsPbBr_3$, the spatial separation of photogenerated carriers in the Z-scheme system allows for an 8.3-fold improvement in photocatalytic performance. Sarkar and colleagues used a hydrothermally produced NiS/RGO nanohybrid film as a Pt-free counter electrode (CE) to construct dye-sensitized solar cell devices with a power conversion efficiency of 9.5% [123]. The enhanced PCE is owing to the synergistic effects of highly catalytic NiS nanoparticles and electrically conductive RGO, which result in the improved electro-catalytic activity of the NiS/RGO nanohybrid for the reduction of triiodide. In comparison to self-assembled conjugate and RGO alone, Joshi et al. [124] produced peptide-functionalized reduced graphene oxide (RGO) nano bioconjugate and observed better antibacterial effectiveness against *Escherichia coli* with much lower cytotoxic activity towards erythrocytes. As a result of these investigations, graphene offers tremendous promise in a variety of nanotechnology applications.

Various graphene-based composites as a photocatalyst and their photocatalytic efficiency towards organic pollutants are tabulated in Table 7.1. The results in Table 7.1 claimed that the ternary composite showed promising efficiency compared to the binary materials or the bare semiconductors. To reach the optimum degradation efficiency, the photocatalyst must be easily synthesizable, cost-effective, solar light activated, feasible reusability, and also removal efficiency within a stipulated time of irradiation.

7.4 Future Prospective

The research on graphene-based heterostructure photocatalysts is still in its infancy stage though graphene-based materials are considered to be one of the most promising photocatalysts for wastewater treatment [125, 126]. There is a huge need for an alternate route of bulk synthesis of 2D-graphene-based heterostructures in a sustainable and cost-effective way. The massive application of this material is predicted to see in industrial wastewater treatment as well as purifying drinking water in the next 5 to 10 years. These materials will be honoured not only for their contributions to

Table 7.1 Comparison of reported graphene-based composites and their degradation efficiency towards different pollutants

Composites and amount	Organic pollutant	Pollutant concentration and total volume	Light source	Irradiation time (min)	Degradation efficiency (%)	Ref
GO/ZnO, 50 mg	MB dye	40 ppm, 50 ml	Sunlight	40	89	[87]
p-type NiO/ n-type GO, 50 mg	MB dye	50 mg/L, 100 ml	500 W mercury-arc lamp	50	97	[85]
TiO_2/Ag_3PO_4/ GO,	RhB dye	20 ppm, 50 ml	250 W tungsten halogen lamp	30	100,	[95]
RGO/TiO_2, 50 mg	Phenol aqueous solution	10 mg/L, 10 ml	Integrated UV light with 2.5 mW/cm^2	-	0.0048 min^{-1}	[103]
Fe_2O_3/RGO, 50 mg	4-Nitrophenol	10 mg/L, 100 ml	Visible light	50	98.0	[105]
ZnO/RGO, 3 mg	MB dye	1×10^{-5} M, 25 ML	100W UV lamp	15	100	[82]
Ag/AgBr/RGO, 25 mg	RhB dye	1×10^{-5} M., 50 ml	250W high-voltage mercury lamp	30	76	[103]
Ag@CdSe-RGO, 50 mg	TC.HCl	20 mg/L, 100 ml	350W Xenon lamp	80	85	[119]
MoO_3/Fe_2O_3/ RGO, 100 mg	MB dye	100 ml	Metal halide lamp (400W)	60	99.47	[109]
RGO/ZnO/Au, 50 mg	Potassium dichromate	10 mg/L, 50 ml	100W Xenon lamp	40	97	[115]
RGO/Fe_2O_3/ g-C_3N_4, 50 mg	Tetracycline (TC) and ciprofloxacin (CP),	20 mg/L, 100 ml each	500W visible irradiation	60	99 and 97	[117]
ZnO-TiO_2/RGO, 20 mg	MB dye	20 mg/L, 100 ml	11 W UV lamp	60	99.7	[113]

3D printing technology, electronics, biotechnology, automobiles, energy production, cosmetics, and sensor technology; but also for their enormous role in the fields of electronics, biotechnology, automobiles, energy production, cosmetics, and sensor technology. However, graphene is still a novel contender in terms of application and it will require substantial processing and patterning technologies. When comparing

graphene to activated carbon, the difference is that graphene does not require post-production functionalization because it has hydroxyl, carboxyl, and epoxide groups on its surface and edges, which let graphene create legendary composites with other semiconductors or metals. Manufacturing a metal-free catalyst will be a wonderful approach to reducing toxicity.

7.5 Conclusions

In conclusion, the versatility of 2D graphene nanosheets in producing composite photocatalysts by connecting with different semiconductors is highlighted in this book chapter. Graphene-based composites can capture photoinduced electrons originating from semiconductor nanoparticles by light illumination. The electrons can be stored in the π–π network of the composites. These electrons can also be travelled to other metal particles deposited on the graphene layer or used to generate active oxygenated radicals. In this way, graphene, GO or RGO retards the electron–hole recombination on semiconducting material as well as extends the absorption of light to longer wavelengths of the visible region. Additionally, GO and RGO can also act as a sensitizer, enhancing the photocatalytic efficiency under visible light irradiation.

The photodegradation of pollutants seems to depend on several factors, such as textural (surface area), chemical and morphological properties of the composites, type of interaction between the composite and the pollutant, and graphene (pure, oxidized, or reduced) content. However, because most of the model pollutants studied so far were dyes (e.g., methylene blue, rhodamine B, rhodamine 6G, methyl orange, and acid orange 7), other classes of pollutants and their photodegradation mechanisms, including emergent contaminants, should be investigated with graphene-based composites. Graphene-based semiconductor composites have shown promise in a variety of applications, including hydrogen generation, sensing, CO_2 reduction, energy storage, antibacterial activity, and self-sterilizing coating. They are, however, still in the early stages of development. More research is needed to create on a wide scale with high reusability for commercial use. Future research should concentrate on the stability of these composites as well as their immobilization on suitable substrates for the continuous operation of photoreactors. Finally, extensive investigation is necessary to develop a superior material for use in device manufacturing.

References

1. Donkova B, Dimitrov D, Kostadinov M, Mitkova E, Mehandjiev D (2010) Mater Chem Phys 123(2–3):563
2. Emil VS, Emily G, Chun-Wei Y (2020) Lancet 396:1285
3. Devi P, Das U, Dalai AK (2016) Sci Total Environ 571:643
4. Michael-Kordatou I, Karaolia P, Fatta-Kassinos D (2018) Water Res 129:208

5. Goswami L, Kumar RV, Pakshirajan K, Pugazhenthi G (2019) J Hazard Mater 365:707
6. Kahl S, Kleinsteuber S, Nivala J, van Afferden M, Reemtsma T (2018) Environ Sci Technol 52(5):2717
7. Dewil R, Mantzavinos D, Poulios I, Rodrigo MA (2017) J Environ Manage 195:93
8. Kumar MS, Sonawane SH, Bethi B (2018) J. Water Process. Eng. 23:250
9. Fu J, Tian Y, Chang B, Xi F, Dong X (2012) J Mater Chem 22:21159
10. Zhao X, Li Z, Chen Y, Zhu Y (2008) Appl Surf Sci 254(6):1825
11. Fujishima A, Honda K (1972) Nature 238(5358):37
12. Yu L, Ding Y, Zheng M (2017) Appl Catal B: Environ 209:45
13. Gao P, Li A, Sun DD, Ng WJ (2014) J Hazard Mater 279:96
14. Di Mauro A, Fragala ME, Privitera V, Impellizzeri G (2017) Mater Sci Semicond Process 69:44
15. Li Z, Zhang Z (2018) J Photochem Photobiol C: Photochem Rev 35:39
16. Tanga J, Zou Z, Ye J (2004) Catal Lett 92:1
17. Mandal SK, Paul S, Datta S, Jana D (2021) Appl Surf Sci 563:150315
18. Remillard J, McBride J, Nietering K, Drews A, Zhang X (2000) J Phys Chem B 104(18):4440
19. Nakamura R, Imanishi A, Murakoshi K, Nakato Y (2003) J Am Chem Soc 125(24):7443
20. Serpone N (1997) J Photochem Photobiol A: Chem 104(1–3):1
21. Tian C, Zhang Q, Wu A, Jiang M, Liang Z, Jiang B et al (2012) Chem Comm 48:2858
22. Thiruvenkatachari R, Vigneswaran S, Moon S (2008) Korean J Chem Eng 25(1):64
23. Sharma M, Jain T, Singh S, Pandey OP (2012) Sol Energy 86:626
24. Zhang Y, Zhang F, Yang Z, Dionysiou DD (2016) J Catal 344:692
25. Sun Q, Wang N, Yu J, Yu JC (2018) Adv Mater 30(45):1804368
26. Huang S, Chen C, Tsai H, Lu C (2018) Sep Purif Technol 197:147
27. Datta S, Singh P, Jana D, Chaudhuri CB, Harbola MK, Johnson DD et al (2020) Carbon 168:125
28. Tan HL, Abdi FF, Ng YH (2019) Chem Soc Rev 48:1255
29. Shang J, Yao W, Zhu Y, Wu N (2004) Appl Catal A 257:25
30. Xiao FX (2012) ACS Appl Mater Interfaces 4:7055
31. Guo J, Li J, Yin A, Fan K, Dai W (2010) Chinese J. Chem. 28:2144
32. Carp O, Huisman CL, Reller A (2004) Prog Solid State Ch 32:33
33. Tamirat AG, Rick J, Dubale AA, Sub W-N, Hwang B-J (2016) Nanoscale Horiz. 1:243
34. Eibner A (1911) Chemiker Zeitung 35:753
35. Coronado MJ, Fresno F, Hernández-Alonso MD, Portela R (2013) Design of advanced photocatalytic materials for energy and environmental applications. Springer, London
36. Kamat PV (2018) ACS Energy Lett 3(6):1394
37. Landau M (1913) C R Chim 156:1894
38. Fujishima A, Honda K (1972) Nature 238:37
39. Ni M, Leung MKH, Leung DYC, Sumathy K (2007) Renew Sustain Energy Rev 11:401
40. Ismail AA, Bahnemann DW (2014) Sol Energy Mater Sol Cells 128:85
41. Fu M, Li Y, Lu SP, Liu J, Dong F (2011) Appl Surf Sci 258:1587
42. Dong M, Zhou P, Jiang C, Cheng B, Yu J (2017) Chem Phys Lett 668:1
43. Wang L, Wang P, Huang B, Ma X, Wang G, Dai Y, et al (2017) Appl Surf Sci 391:557
44. Ullah R, Dutta J (2008) J Hazard Mater 156:194
45. Hoffmann MR, Martin ST, Choi W, Bahnemann DW (1995) Chem Rev 95:69
46. Wan X, Liang X, Zhang C, Li X, Liang W, Xu H et al (2015) Chem Eng J 272:58
47. Sun S, Chang X, Li X, Li Z (2013) Ceram Int 39:5197
48. Wu C (2014) Appl Surf Sci 319:237
49. Qin H, Li W, Xia Y, He T (2011) ACS Appl Mater Interfaces 3:3152
50. Samadi M, Shivaee HA, Zanetti M, Pourjavadi A, Moshfegh AZ (2012) J Mol Catal A Chem 359:42
51. Ma X (2011) J Nanomaterials 2011:952616
52. Zhou Y, Chen G, Yu Y, Feng Y, Zheng Y, He F et al (2015) Phys Chem Chem Phys 17:1870
53. Lin YG, Hsu YK, Chen YC, Chen LC, Chen SY, Chen KH (2012) Nanoscale 4:6515

54. Wang F, Liang L, Shi L, Liu M, Sun J (2014) Dalton Trans 43:16441
55. Fan SW, Yao KL, Liu ZL (2009) Appl Phys Lett 94:52506
56. Sun Y, He T, Guo H, Zhang T, Wang W, Dai Z (2010) Appl Surf Sci 257:1125
57. Patil AB, Patil KR, Pardeshi SK (2010) J Hazard Mater 183:315
58. Yu W, Zhang J, Peng T (2016) Appl Catal B: Environ 181:220
59. Muruganandham M, Kusumoto Y (2009) J Phys Chem C 113:16144
60. Liu S, Li C, Yu J, Xiang Q (2011) Cryst Eng Comm 13:2533
61. Kang HW, Leem J, Sung HJ (2015) RSC Adv 5:51
62. Vaiano V, Matarangolo M, Murcia JJ, Rojas H, Navío JA, Hidalgo MC (2018) Appl Catal B: Environ 225:197
63. Chen LT, Liao UH, Chang JW, Lu SY, Tsai DH (2018) Langmuir 34:5030
64. Jung S, Yong K (2011) Chem Comm 47:2643
65. Bharathia P, Harisha S, Archana J, Navaneethan M, Ponnusamy S, Muthamizhchelvan C et al (2019) Appl Surf Sci 484:884
66. Ranjith KS, Kumar DR, Huh YS, Han YK, Uyar T, Kumar RTR (2020) J Phys Chem C 124:3610
67. Novoselov KS, Geim AK, Morozov SV, Jiang D, Zhang Y, Dubonos SV et al (2004) Science 306:666
68. White RL, White CM, Turgut H, Tian ZR (2018) J Taiwan Inst Chem Eng 85:18
69. Bolotin KI, Sikes KJ, Hone J, Stormer HL, Kim P (2008) Phys Rev Lett 101:1
70. Geim AK (2009) Science 324(1530)
71. Zhang S, Wang H, Liu J, Bao C (2020) Mater Lett 261:127098
72. Jiang HB, Zhang YL, Zhang Y, Liu Y, Fu XY, Liu YQ et al (2015) Sci Rep 5:17522
73. Ni J, Li Y (2016) Adv Energy Mater 6:1600278
74. Li Z, Liu Z, Sun H, Gao C (2015) Chem Rev 115:7046
75. Kim KS, Zhao Y, Jang H, Lee SY, Kim JM, Kim KS et al (2009) Nature 457(7230):706
76. Wang B, Feng W, Zhang L, Zhang Y, Huang X, Fang Z et al (2017) Appl Catal B: Environ 206:510
77. Dideikin AT, Vul AY (2019) Front Phys 6:149
78. Paredes JI, Villar-Rodil S, Solís-Fernández P, Martínez-Alonso A, Tascon JMD (2009) Langmuir 25:5957
79. Wang J, Zhang J, Han L, Wang J, Zeng H (2021) Adv Colloid Interface Sci 289:102360
80. Deshpande RH, Wasif AI, Shah K (2019) Int Res J Eng Technol 06(06):1886
81. Dreyer DR, Park S, Bielawski CW, Ruoff RS (2010) Chem Soc Rev 39:228
82. Mandal SK, Dutta K, Pal S, Mandal S, Naskar A, Pal PK et al (2019) Mater Chem Phys 223:456
83. Lin C, Gao Y, Zhang J, Xue D, Fang H, Tian J et al (2020) J Mater Res 35:1307
84. Durmus Z, Kurt BZ, Durmus A (2019) ChemistrySelect 4:271
85. Ahmad J, Majid K, Dar MA (2018) Appl Surf Sci 457:417
86. Gao P, Liu J, Sun DD (2013) W. Ng. J Hazard Mater 250:412
87. Sharma M, Sondhi H, Krishna R, Srivastava SK, Rajput P, Nigam S, Joshi M (2020) Environ Sci Pollut Res 27:32076
88. Chen H, Ji W, Gu M, Li Y, Cheng X (2021) J Mater Sci 32:27564
89. Sahu BK, Juine RN, Sahoo M, Kumar R, Das A (2021) Chemosphere 276:130142
90. Abhilasha MR, Srikantaswamy S (2018) Int J Res Anal Rev 5:27
91. Rajachandrasekar T, Selvakumar P, Balakrishnan K (2016) J Environ Nanotechnol 5(2):04
92. Vinoth R, Neppolian B (2014) Mater Focus 3:485
93. Moral-Rodríguez A, Quintana M, Leyva-Ramos R (2022) Ceram Int 48:1264
94. Chen W, Niu X, Wang J (2018) J Photochem Photobiol A 356:304
95. Lu B, Ma N, Wang Y, Qiu Y, Hu H, Zhao J, Liang D, Xu S, Li X, Zhu Z, Cui C (2015) J Alloys Compd 630:163
96. Yang X, Qin J, Jiang Y, Chen K, Yan X, Zhang D, Li R, Tang H (2015) Appl Catal B Environ 166:231
97. Qin J, Li R, Lu C, Jiang Y, Tang H, Yangn X (2015) Ceram Int 41:4231

98. Jo W-K, Selvam NCS (2015) J Hazard Mater 299:462
99. Bai Y-Y, Wang F-R, Liu J-K (2016) Ind Eng Chem Res 55:9873
100. Kausor MA, Chakrabortty D (2020) Inorg Chem Commun 116:107907
101. Dai K, Lu L, Liang C, Zhu G, Liu Q, Geng L, He J (2015) Dalton Trans 44:7903
102. Alamgholiloo H, Rostamnia S, Zhang K, Lee TH, Lee Y-S, Varma RS, Jang HW, Shokouhimehr M (2020) ACS Omega 5:5182
103. Wang P, Wang J, Wang X, Yu H, Yu J, Lei M, Wang Y (2013) Appl Catal B Environ 132–133:452
104. Lellala Kashinath K, Namratha KB (2017) J Alloys Compd 695:799
105. Mohan BS, Ravi K, Anjaneyulu RB, Sree GS, Basavaiah K (2019) Physica B Condens Matter 553:190
106. Gnanamoorthy G, Yadav VK, Latha D, Karthikeyan V, Narayanan V (2020) Chem Phys Lett 739:37050
107. Choudhari A, Bhanvase BA, Saharan VK, Salame PH, Hunge Y (2020) Ceram Int 46(8):11290
108. Dashairya L, Sharma M, Saha P (2019) J Alloys Compd 774:625
109. Anjaneyulu RB, Mohan BS, Naidu GP, Muralikrishna R (2018) J Asian Ceram Soc 6(3):183
110. X-h Meng X, Shao H-y, Yin J, Wang J, Liu F-z, X-h Liu M, Wang H-L (2013) Mater Lett 105:162
111. Jing Z, Dai X, Xian X, Zhang Q, Zhong H, Li Y (2020) Materials 13:2529
112. Dutta S, Sahoo R, Ray C, Sarkar S, Jana J, Negishi Y, Pal T (2015) Dalton Trans 44:193
113. Viet TQQ, Khoi VH, Giang NTH, Anh HTV, Dat NM, Phong MT, Hieu NH (2021) Colloids Surf A Physicochem Eng Asp 629:127464
114. Guan Z, Wang P, Li Q, Li Y, Fu X, Yang J (2017) Chem Eng J 327:397
115. Xia Y, Gang R, Xu L, Huang S, Zhou L, Wang J (2020) Ceram Int 46:1487
116. Hu X, Deng F, Huang W, Zeng G, Dionysiou DD (2018) Chem Eng J 350:248
117. Shanavas S, Mohana S, Roopan A, Priyadharsan D, Devipriya S, Jayapandi RA, Anbarasan PM (2019) Appl Catal B Environ 255:117758
118. Ding J, Liu L, Xue J, Zhou Z, He G, Chen H (2016) J Alloys Compd 688:649
119. Zhou M, Li J, Ye Z, Ma C, Wang H, Huo P, Shi W, Yan Y (2015) ACS Appl Mater Interfaces 7:28231
120. Sadeghzadeh-Attar A (2020) J Taiwan Inst Chem Eng 111:325
121. Hu X, Zhao Y, Wang H, Cai X, Hu X, Tang C, Liu Y, Yang Y (2018) J Chem Technol Biotechnol 93:2226
122. Jiang Y, Liao J-F, Chen H-Y, Zhang H-H, Li J-Y, Wang X-D, Kuang D-B (2020) Chem 6:766
123. Sarkar A, Chakraborty AK, Bera S (2018) Sol Energy Mater Sol Cells 182:314
124. Joshi S, Siddiqui R, Sharma P, Kumar R, Verma G (2020) Sci Rep 10:9441
125. Kumar A, Hasija V, Sudhaik A, Raizada P, Nguyen V-H, Le QV et al (2022) Environ Res 209:112814
126. Kumar P, Dhand C, Dwivedi N, Singh S, Khan R, Verma S et al (2022) Renew Sustain Energy Rev 157:111993
127. Coping with water scarcity, Challenge of the twenty-first century, UN-Water, FAO, 2007